The Journal of Chemical Physics ARTICLE pubs.aip.org/aip/jcp

Anomalous segmental dynamics of supercooled polyrotaxane melts: A computer simulation study

Cite as: J. Chem. Phys. 159, 244901 (2023); doi: 10.1063/5.0180375
Submitted: 9 October 2023 • Accepted: 4 December 2023 •
Published Online: 22 December 2023

Xiang-Meng Jia[1,2] and Jiajia Zhou[1,2,a)]

AFFILIATIONS

[1] South China Advanced Institute for Soft Matter Science and Technology, School of Emergent Soft Matter, South China University of Technology, Guangzhou 510640, China
[2] Guangdong Provincial Key Laboratory of Functional and Intelligent Hybrid Materials and Devices, South China University of Technology, Guangzhou 510640, China

[a)] **Author to whom correspondence should be addressed:** zhouj2@scut.edu.cn

ABSTRACT

Polyrotaxanes, which consist of mechanically interlocked bonds with rings threaded onto soft polymer chains, exhibit unique mechanical properties and find applications in diverse fields. In this study, we investigate the anomalous segmental dynamics of supercooled polyrotaxane melts using coarse-grained molecular dynamics simulations. Our simulations reveal that the presence of rings effectively reduces the packing efficiency, resulting in well-contained local motion even below the glass transition temperature. We also observe variations in dynamical free volume, characterized by the Debye–Waller factor, which shows a minimum at a ring coverage of 0.1 on threading chains. Such a non-monotonic dependence on coverage shows great consistency in structural relaxation time and dynamic heterogeneity. Specifically, the high segmental mobility of threading linear chains at large coverage can be attributed to the increased dynamical free volume due to supported rigid rings. However, such anomalous segmental dynamics is limited to length scales smaller than one ring size. Beyond this characteristic length scale, the diffusion is dominated by topological constraints, which significantly reduce the mobility of polyrotaxanes and enhance the dynamic heterogeneity. These findings offer microscopic insights into the unique packing structures and anomalous segmental dynamics of supercooled polyrotaxane melts, facilitating the design of advanced materials based on mechanical interlocking polymers for various applications.

I. INTRODUCTION

Mechanically interlocked molecules (MIMs), also known as mechanical interlocking polymers, have received significant attention in the field of materials science due to their unique molecular architectures and exceptional mechanical properties.[1–4] Among these MIMs, polyrotaxanes stand out as a class of materials composed of cyclic molecules threaded onto linear polymer chains, resulting in a mechanically interlocked structure. This threading interaction imparts polyrotaxanes with distinctive characteristics, such as mechanical robustness, stimuli-responsiveness, and dynamic behavior, which make them suitable for various applications in nanotechnology,[5–7] biomedicine,[8–11] and materials engineering.[12–15]

In recent years, there has been a surge of interest in polyrotaxane glass-forming materials,[16–22] in which cyclodextrins (CDs) have been widely used for the inclusion of complex formation with linear polymers. The hydroxyl groups on the exterior surface of the truncated cone of CDs can form cooperative hydrogen bonds. By introducing bulky substituents or altering the functional groups, the ability to form hydrogen bonds is attenuated, reducing the likelihood of material crystallization.[18] Kato and coworkers[16] demonstrated an unusually broad glass transition phase, which can be attributed to segmental motion, which is unresponsive to cooperative motion with neighboring chains until the vitrification process is completed. Remarkably, even in the glass state, the threading linear polymers maintain high mobility within the porous glassy framework. This anomalous mobility of the polymer chains results in the emergence of strong sub-relaxations, ultimately altering the material's elastic modulus significantly. In a recent study on the toughening mechanism in ductile polyrotaxane glassy materials,[23] it was discovered that the unique interlocking constraints can lead to a significantly harder reconstructed structure during the straining process, resulting in a stable propagation of necking.

There are primarily two approaches for modifying the mechanical properties of polyrotaxane glass-forming materials. The first approach involves adjusting structural parameters, such as the ring size. Increasing the ring size can effectively weaken topological constraints and enhance the steepness of the glass transition region.[20] The second approach involves manipulating chemical interactions between the host rings and the threading guest polymer. For example, increasing the interaction strength between the host rings and the threading guest polymer can enhance the sliding friction of the rings and decrease the mobility of the threading chains.[19] All of these methods are related to the structural packing and segmental dynamics of polyrotaxanes. Thus, understanding the microscopic structural origin of anomalous dynamics of polyrotaxanes is crucial for unlocking their full potential. Computer simulations have played a pivotal role in material science, enabling us to unravel the underlying mechanisms at the atomistic level and facilitating the design of novel materials. However, current relevant studies mainly focus on properties above the glass transition temperature, such as the sliding dynamics of rings on axial chains.[24,25] Therefore, a comprehensive investigation of the structure and dynamics of polyrotaxanes in the supercooled state is warranted.

Motivated by the aforementioned challenges, we employ coarse-grained molecular dynamics simulations to investigate the atypical segmental dynamics as well as the microscopic structures of supercooled polyrotaxane melts with varying ring coverage. Through an in-depth exploration of the interplay between the rings and the threading linear chains, our objective is to unravel the underlying structural origins of subrelaxations and cooperative motion. The findings obtained from this research will contribute significantly to a comprehensive understanding of the intricate dynamics exhibited by polyrotaxanes. Ultimately, these insights will pave the way for the development of advanced materials with precisely tailored mechanical properties and wide-ranging applications. This article is organized as follows: Sec. II provides a detailed description of the simulation methods employed. Section III presents the results pertaining to the structure and dynamic properties of the simulated systems. Finally, the conclusions derived from this study are summarized in Sec. IV.

II. SIMULATION METHODS AND DETAILS

In our simulation, the bead spring model is used to represent the polymers and ring molecules, which is widely used in the investigation of polymer glass formation.[26–28] To keep the chain connectivity, the interactions between bonded pair beads are described by the finitely extensible nonlinear elastic (FENE) potential,

$$U(r) = -\frac{1}{2}kr_0^2 \ln\left[1 - \left(\frac{r-\Delta}{r_0}\right)^2\right] + U_{\mathrm{WCA}}(r), \tag{1}$$

where

$$U_{\mathrm{WCA}}(r) = \begin{cases} \varepsilon\left[\left(\frac{\sigma}{r-\Delta}\right)^{12} - \left(\frac{\sigma}{r-\Delta}\right)^{6}\right] + \varepsilon, & r-\Delta < 2^{\frac{1}{6}}\sigma, \\ 0, & r-\Delta \geq 2^{\frac{1}{6}}\sigma, \end{cases} \tag{2}$$

and k and r_0, with the common choices of $k = 30\varepsilon/\sigma^2$ and $r_0 = 1.5\sigma$, correspond to the attractive force strength and maximum size of the bond, respectively. Here, r represents the instantaneous length of the bond, and ε and σ denote the energy and length scales, respectively. The radial shift value Δ is defined by the diameters of two bonded beads with an arithmetic mean $(d_i + d_j)/2 - \sigma$. In order to prevent the release of rings from a threaded polymer chain, the diameter of the terminal beads is set to 2.0σ, while the remaining beads have a diameter of 1.0σ. To maintain the planar structure of the ring molecule consisting of eight connected beads, a harmonic angle potential is applied.

$$U(\theta) = \frac{1}{2}k(\theta - \theta_0)^2, \tag{3}$$

where θ denotes the included angle between the adjacent bond and the equilibrium angle θ_0 is set to $3\pi/4$. The angle strength k is set to $300\varepsilon/\sigma^2$. Finally, the nonbonded interactions between any nonbonded pair beads are modeled through truncated-and-shifted Lennard–Jones (LJ) potential,

$$U^{\mathrm{LJ}}(r) = 4\varepsilon\left[\left(\frac{\sigma}{r-\Delta}\right)^{12} - \left(\frac{\sigma}{r-\Delta}\right)^{6}\right] + C(r_{\mathrm{cut}}), \tag{4}$$

where r is the distance between two beads. The interaction range r_{cut} is set to 2.5σ to include attractive force, which is a common choice in simulating glassy materials.[29–31] $C(r_{\mathrm{cut}})$ is a shift constant to guarantee that potential smoothly goes to zero at r_{cut}. The standard reduced units were used, with $\sigma = \varepsilon = m = 1$ and time scale $\tau = (\sigma^2 m/\varepsilon)^{0.5}$.

The polymerization degree M of the linear chain in polyrotaxane is 120. As depicted in Figs. 1(a) and 1(b), the coverage ϕ is defined as the number of rings n to the chain length M in one polyrotaxane chain, i.e., $\phi = n/M$. We roughly map the length scale $\sigma = 1.0$ nm, which is comparable to the size of two consecutive PEG units. In pioneering experiments of polyrotaxanes composed of polyethylene glycol (PEG) and α-CD,[18,32] the full coverage of the rings on threading polymer corresponding to $\phi = 1.0$ is defined when CD:repeating unit is 1:2. In our simulation, one bead stands for two PEG units, and therefore, the definition of coverage ϕ aligns with that employed in experimental investigations. We filled the simulation box with 100 polyrotaxanes, with ϕ ranging from 0.0 to 0.3. All the simulations were performed by the GALAMOST dynamics simulation package[33] in a cubic box with periodic boundary conditions, and the integration timestep $\Delta t = 0.001$ was used. First, we built the simulated system with a low number density $\rho = 0.1$. The

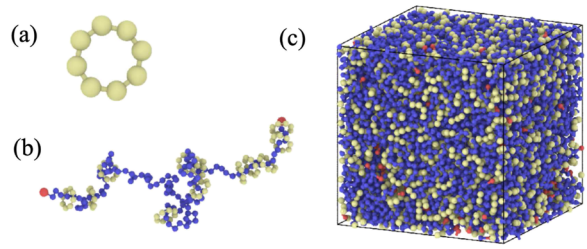

FIG. 1. (a) A cartoon of one single ring with eight beads. (b) One polyrotaxane chain consisting of one linear chain with polymerization degree $M = 120$ and rings threaded with the coverage $\phi = 0.1$. (c) A Snapshot of the simulated system consisting of 100 polyrotaxane chains.

equilibrated system was obtained through an NPT simulation with $P = 0.1\varepsilon/\sigma^3$ for $2 \times 10^5\tau$ at $T = 1.5$, followed by an NVT simulation for $2 \times 10^5\tau$. In this equilibration stage, the center of mass of all simulated PR diffused for at least ten times of its radius of gyration (R_g). Subsequently, the equilibrated melt was subjected to a stepwise cooling process from $T = 1.5$ to $T = 0.1$ at a rate of $10^{-4}\varepsilon/(k_B\tau)$, with fixed pressure $P = 0.1\varepsilon/\sigma^3$. At each temperature, the system was further equilibrated by another NVT simulation for $2 \times 10^5\tau$. Finally, the NVT production run for $10^5\tau$ was carried out for data analysis.

III. RESULTS AND DISCUSSION

We begin by examining the thermodynamic properties. The specific volume V_{sp}, defined as the reciprocal of the number density ρ, is employed to estimate the glass transition temperature (T_g). This is accomplished by extrapolating the linear regime of V_{sp} for both the liquid and glassy regions (see Fig. S1). The results presented in Fig. 2 indicate that the rigid rings can enhance the T_g of linear polymer melts, while reaching a plateau at high coverages. This is consistent with experimental observations[17,18] that the T_g of polyrotaxanes, comprising threading PEG chains and methoxyethylated α-CD ($\phi^{exp} = 0.25$), is raised by ~60 K in comparison to linear PEG melts. To illustrate the structural packing, we also display the number density ρ at $T = 0.55$, which exhibits a steep decrease with increasing ϕ up to 0.1, followed by a nearly linear decline for larger ϕ. To clearly show the packing structure, we calculated the partial coordination number n_p for central linear or ring monomers surrounded by linear or ring monomers. Note that we examined three types of n_p, that is, "linear–linear," "linear–ring," and "ring–ring" types, with the first term indicating the centers and the latter for surrounding monomers. The value of n_p was obtained by integrating the density distribution $\rho(r)$ (see Fig. S2),

$$n_p = 4\pi \int_0^{r_1} r^2 \rho(r) dr, \tag{5}$$

where r is the distance and $r_1 = 1.5\sigma$ is the location of the first minimum. As shown in Fig. 2(b), the averaged coordination number, denoted as n_p, exhibits a significant rise in the "linear–ring" type systems with coverage below $\phi < 0.1$. However, as the coverage increases, the rate of increase gradually diminishes. Such an increasing trend is the same for "ring–ring" n_p. Note that the polyrotaxane chain is composed of rigid rings and soft linear chains. Such a mismatch in molecular stiffness can significantly decrease the local packing efficiency of their blends. Moreover, the "linear–linear" n_p shows an obvious decrease with ϕ, especially for systems with $\phi < 0.1$. It demonstrates that the threading linear chains are separated from neighboring chains, and the packing structures show minor change above the critical point with $\phi = 0.1$. Even though these thermodynamic properties provide us the insights into structural packing, we cannot rationalize the unique dynamics derived from topological constraints between rings and threading chains. As articulated by Kato and coworkers,[17] polyrotaxanes, featuring mechanically interlocked bonds, cannot be regarded merely as a simple blend due to their distinctive mechanical properties associated with segmental relaxation. Therefore, our subsequent focus centers on characterizing dynamics properties.

To characterize the segmental dynamics, we calculated the structural relaxation of linear chains by analyzing the self-part of the intermediate scattering function,

$$F_s(q,t) = \frac{1}{N}\left\langle \sum_{j=1}^{N} \exp\{-i\mathbf{q}\cdot[\mathbf{r}_j(t) - \mathbf{r}_j(0)]\}\right\rangle, \tag{6}$$

where $\mathbf{r}_j$ represents the position of particle j at time t, $\mathbf{i}$ is the imaginary unit, $q = |\mathbf{q}|$ is the wave number, and $\langle \dots \rangle$ denotes ensemble average. The wave number was chosen to be $q = q^* = 7.0\sigma^{-1}$, which corresponds to the location of the main peak of the static structure factor. This particular choice of q indicates that we are examining relaxation at the segmental level. Figure 3(a) shows the time dependence of $F_s(q,t)$ for simulated systems with different coverages at $T = 0.55$. The stretching in the final decay is related to the so-called "dynamical heterogeneities (DH)." Interestingly, our simulations at $T = 0.55$ indicate that such a stretching regime intensifies from linear chain melts to polyrotaxane melts with ϕ up to 0.1 while gradually disappearing at high coverage ϕ. To quantify the effect of coverage, we defined the structural relaxation time τ_α as the time at which $F_s(q,t)$ decays to 0.2, which is a common choice in studying glass-forming materials.[29,34,35] Intuitively, the threading linear chains are topologically constrained by rings, which is more pronounced with the increase in ϕ. As a consequence, it is expected that the segmental structural relaxation time τ_α of the linear chains will also increase as ϕ increases. However, as shown in Fig. 3(b), τ_α reaches its maximum at approximately $\phi = 0.1$ and subsequently decreases with a further increase in ϕ. It demonstrates that the segmental structural relaxation of linear chains in systems with large coverage ($\phi > 0.1$) is actually accelerated rather than slowed down. This dependence becomes more noticeable at lower temperatures. Furthermore, it is important to note that T_g for all polyrotaxane

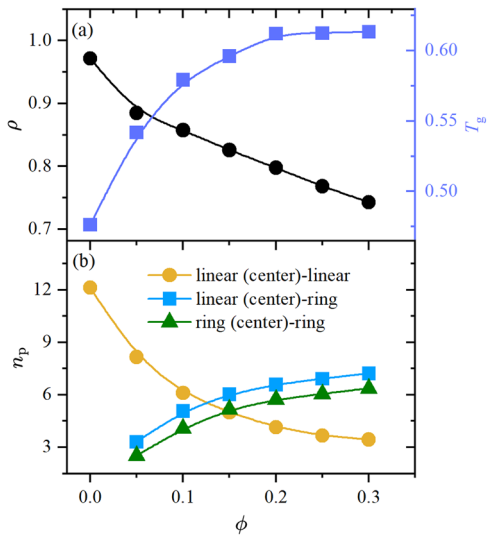

FIG. 2. (a) The total number density ρ at $T = 0.55$ and T_g of simulated systems as a function of coverage ϕ. (b) The partial coordination number n_p for central monomers of linear or ring monomers surrounded by linear or ring monomers (linear–linear, linear–ring, and ring–ring types) as a function of coverage ϕ. The solid lines are just guides for the eyes.

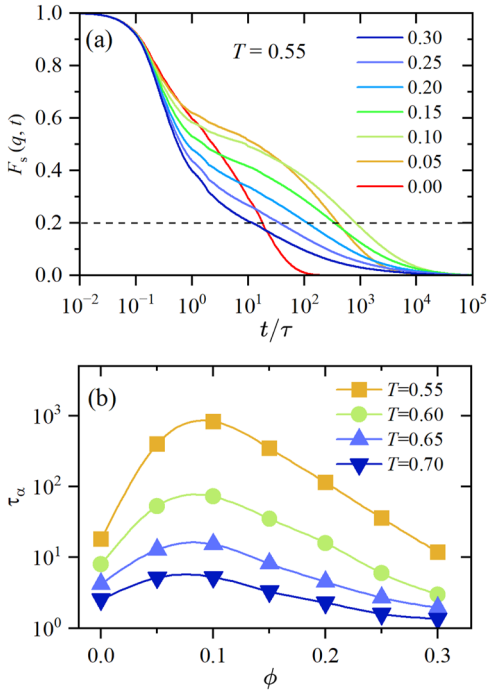

FIG. 3. (a) Self-part of the intermediate scattering function $F_s(q, t)$ in systems with different coverage ϕ ranging from 0.0 (linear polymer melts) to 0.3 at $T = 0.55$. (b) Logarithm structural relaxation time τ_α as a function of coverage ϕ at different temperatures. The solid lines are just guides for the eyes.

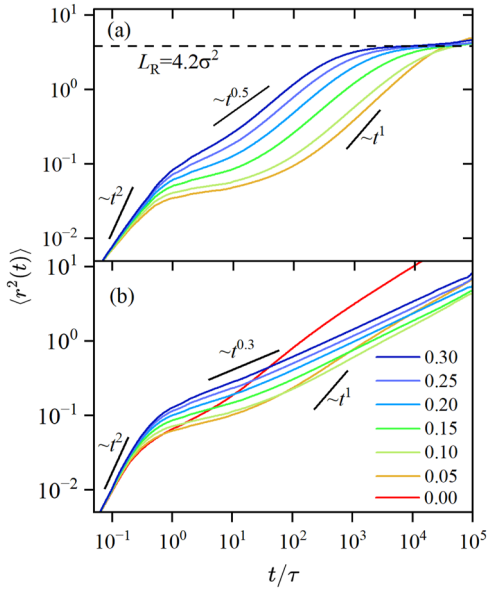

FIG. 4. The mean squared displacement in simulated systems with different coverages for (a) monomers of rings and (b) monomers of linear chains at $T = 0.55$ for systems with a series of coverage $\phi = 0.0$–0.3. The short solid lines are for scaling factors in $\langle r^2(t) \sim t^v \rangle$.

melts in this simulation falls in the range of 0.542–0.617 (see Fig. 2), indicating that most of our simulated systems are in glassy state at investigated temperatures ($T = 0.5$–0.7). Different from conventional polymer melts being frozen under T_g, the linear chains in glassy polyrotaxane melts show fast relaxation, especially at systems with large coverage. Such strong subrelaxation in the glassy state of polyrotaxane melts is also observed in experiments.[18] These findings imply that the mechanical interlocking bonds between linear chains and rings can significantly change the local packing structures and, hence, the dynamics. Next, we considered characterizing the diffusion behaviors of rigid rings and threading chains as well as free volume to grasp the microscopic origin of the observed anomalous local dynamics.

In order to characterize the segmental diffusion, we calculated the mean square displacement (MSD) $\langle r^2(t) \rangle$, which is defined by

$$\langle r^2(t) \rangle = \frac{1}{N} \left\langle \sum_{j=1}^{N} |\mathbf{r}_j(t) - \mathbf{r}_j(0)|^2 \right\rangle, \tag{7}$$

where $\mathbf{r}_j$ represents the position of monomer j at time t and $\langle \dots \rangle$ denotes the ensemble average. The MSD scales over time as $\langle r^2(t) \sim t^v \rangle$, where v denotes the scaling factor. At short times, the monomers exhibit unimpeded motion without any particle collisions, characterized by ballistic diffusion ($\sim t^2$). As time progresses, the motion becomes increasingly influenced by particle collisions, resulting in monomers being confined by neighboring particles, indicating a subdiffusive regime ($\sim t^v$ where $v < 1$). Figure 4(a) displays the MSD of monomers in rings for simulated systems at $T = 0.55$ with different coverages. Interestingly, the MSD data for all systems with different coverages reach a plateau denoted as L_R at $\sim 4.2\sigma^2$, resembling the size of one single ring. This plateau is illustrated by a horizontal dashed line in the figure. This distinctive length scale L_R effectively separates the MSD into two distinct regimes. Within the first regime, characterized by the MSD smaller than L_R, the ring monomers are accelerated as ϕ increases. As aforementioned, the packing density experiences a steep decrease as ϕ increases up to 0.1, followed by a nearly linear decline with further increases in ϕ. The fraction of ring monomers within the simulated systems increases rapidly as ϕ increases, leading to the dominance of ring structures in determining the local packing arrangements. Hence, the local packing efficiency significantly decreases as ϕ increases, resulting in an enhanced mobility of ring monomers. Conversely, within the second regime, where the MSD exceeds L_R, the motion of ring monomers decelerates with increasing ϕ. This reversal in the mobility of ring monomers around the characteristic length scale L_R becomes more noticeable at higher temperatures (see Fig. S3). Within this regime, the diffusion of polyrotaxane is dictated by the topological constraints that arise from mechanically interlocked bonds formed between the rings and linear chains. Figure 4(b) represents the diffusion of monomers in linear chains. Monomer mobility exhibits a non-monotonic behavior as ϕ increases. Additionally, the scaling factor $v = 0.3$ remains consistent throughout the entire simulation period except for the very early stage, for systems with significant coverage, such as $\phi = 0.3$, suggesting a form of pseudo-ballistic diffusion. The findings presented above are consistent with experimental observations that indicate

secondary relaxation dynamics in polyrotaxane melts at the glassy state.[17,18] The rigidity of the rings is anticipated to provide additional "free volume" for the linear chains. However, due to the potentially perplexing nature of this concept, we aim to quantify this parameter in subsequent calculations.

Instead of relating the local density with the molecular mobility, we characterize free volume using a dynamical method. As proposed by Douglas and coworkers,[28,36,37] the Debye–Waller factor $\langle u^2 \rangle$, a measure of rattle-space, can be calculated from the MSD of polymer segments at caging time, which is strongly related to mobility. In our simulation, we defined this caging time with $t = 100\tau$. It is important to note that this quantity is typically a small value like 1τ, corresponding to particle vibrations from the idealized positions,[34,38] while in this simulation, we focus on the diffusion of linear chains confined in the free space supported by rigid rings, and hence, the time scale of such vibrations is different from the common choice. Figure 5 gives the $\langle u^2 \rangle$ of linear chains as a function of coverage at different temperatures. The results demonstrate that the free volume for linear chains decreases with the increase in coverage compared to pristine linear melts, reaches a minimum at about $\phi = 0.1$, and then increases with larger ϕ. Such a dependence is more pronounced at high temperatures. The results are in good agreement with structural relaxation times, which reach a maximum at the same ϕ at which $\langle u^2 \rangle$ reaches the minimum. Combining the data of free volume and the partial coordination number in Fig. 2(b), we can relate such a change in free volume with structural packing. Threading a small fraction of rigid rings onto linear chains cannot well screen the intermolecular interactions, and the bulky rigid rings slow down the structural relaxation at the same time. However, with enough coverage ϕ, the local structural packing efficiency is significantly decreased. As shown in the inset of Fig. 5, the linear chains in polyrotaxane with $\phi = 0.3$ are confined in a "one-dimensional" tunnel created by rigid rings. In this case, the linear chains are separated from other polyrotaxane chains. Therefore, the local relaxation of threading chains inside the network of rigid rings remains isolated and will never transform into a glassy state due to the "frozen free volume" provided by neighboring rigid rings, even at temperatures well below T_g.

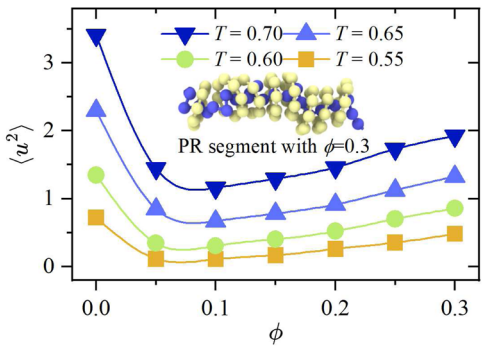

FIG. 5. The Debye–Waller factor $\langle u^2 \rangle$ of linear chains as a function of coverage ϕ ranging from 0.05 to 0.3 at different temperatures. The solid lines are just guides for the eyes. The inset shows a snapshot of one polyrotaxane segment in simulated systems with $\phi = 0.3$.

The rigid rings in polyrotaxane effectively screen the intermolecular contacts for threading chains, confining them in the space supported by rings as shown in the inset of Fig. 5. The mobility of caged monomers is determined by the amount of free volume available to explore, which is directly related to the DH. Here, we aim to characterize DH of linear chains through the non-Gaussian parameter,

$$\alpha_2 = \frac{3\langle r^4(t) \rangle}{5\langle r^2(t) \rangle^2} - 1, \tag{8}$$

where $r(t)$ denotes the displacement of a particle in threading chains and $\langle \cdots \rangle$ represents the ensemble average. This parameter describes the DH exhibited by mobile particles, which dominate molecular diffusion that enables structural relaxation and collective motion.[34] As shown in Fig. S5, the $\alpha_2(t)$ parameter is nearly zero at short time regimes and exhibits a primary peak at time t^*, which directly relates to the lifetime of mobile particle clusters. The peak value L_{α_2} and the corresponding peak time τ_{α_2} are summarized in Fig. 6, which can be used to characterize the spatially heterogeneous motion of the mobile particles. The results indicate the same dependence on coverages and temperatures compared to structural relaxation time (see Fig. 3) and a reverse one compared to free volume (Fig. 5). Douglas and coworkers[38] demonstrated a reverse correlation between the local dynamic free volume and the growth of collective motion in supercooled liquids, while in our simulations, such relations are restricted on the time scales of structural relaxation. As shown in Fig. S5, there is a second DH peak at long time scales, which is more pronounced for systems with high coverage. The second DH peak of linear chains can be attributed to the mobile heterogeneity on length scale larger than L_R. It is expected that α_2 will decay to zero

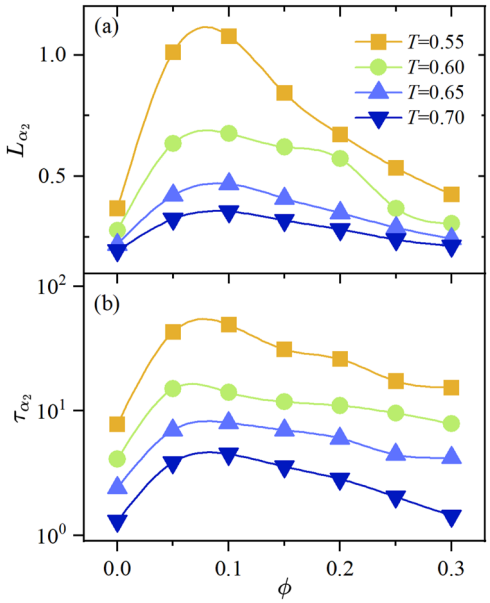

FIG. 6. (a) The peak value of non-Gaussian parameter $L_{\alpha 2}$ and (b) corresponding time τ_{α_2} as a function of coverage ϕ at different temperatures. The solid lines are just guides for the eyes.

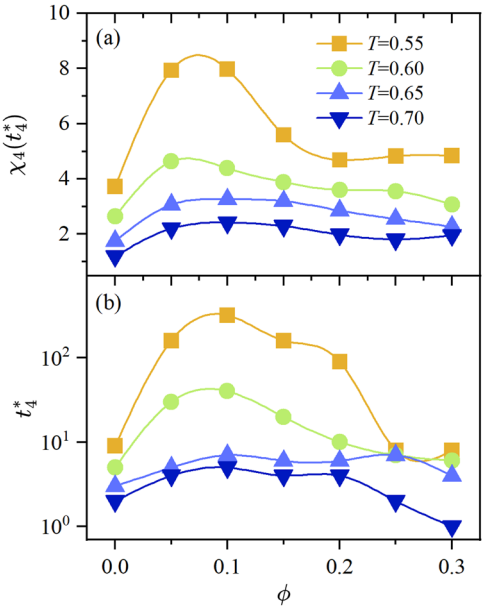

FIG. 7. (a) The peak value of four-point susceptibility χ_{χ_4} and (b) corresponding time τ_{χ_4} as a function of coverage ϕ at different temperatures. The solid lines are just guides for the eyes.

at the relaxation times of the whole polyrotaxane chain, which is beyond the computational ability in our simulation at temperatures near T_g.

Finally, as a complement to the non-Gaussian parameter, we seek to quantify DH of linear chains from the perspective of immobile particles by calculating the four-point susceptibility $\chi_4(t)$,

$$\chi_{4,\,s}(t) = \frac{V}{N^2}\left[\langle Q_s(t)^2\rangle - \langle Q_s(t)\rangle^2\right], \tag{9}$$

where V is the volume, N is the number of particles, and $\langle\cdots\rangle$ denotes the ensemble average. Here, $Q_s(t)$ is a dynamic order parameter defined by an overlap function,

$$Q_s(t) = \sum_{i=1}^{N} w(|\mathbf{r}_i(0) - \mathbf{r}_i(t)|), \tag{10}$$

where $w = 1$ for $|\mathbf{r}_i(0) - \mathbf{r}_i(t)| < 0.3\sigma$ and zero otherwise and the summation runs over all N particles. Figure S6 shows the dynamical susceptibility $\chi_4(t)$ as a function of time at different temperatures. As shown in Fig. S5, $\chi_4(t)$ is zero at short times and has a maximum at intermediate time t_4^*. The peak value $\chi_4(t_4^*)$ is closely related to dynamic correlations, which can be used to quantify the length scales of DH.[39] The characteristic values $\chi_4(t_4^*)$ and t_4^* shown in Fig. 7 indicate a similar dependence on coverage compared to structural relaxation time, non-Gaussian parameter. Note that such a dependence disappears on the time scales beyond the relaxation time of one single ring, which is in good agreement with α_2 versus time.

IV. CONCLUSIONS

In this study, we conducted coarse-grained molecular dynamics simulations to explore the segmental dynamics of supercooled polyrotaxane melts with varying coverage ϕ from 0.0 to 0.3. The incorporation of rigid rings was discovered to have a profound influence on the packing efficiency and dynamic behavior of the polymer chains.

Our simulations reveal that the introduction of rigid rings onto linear chains through mechanically interlocked bonds effectively reduces the local packing efficiency, leading to rapid local relaxation. The hollow structure of the rings allows the monomers of threaded linear chains to explore additional local free space. By quantifying the rattle-space of linear chains using the Debye–Waller factor $\langle u^2\rangle$, we were able to determine the dynamical free volume. Our results demonstrate that a minimum ring coverage of $\phi = 0.1$ is required for effective screening. As coverage ϕ increases from 0.1, the structural packing of rigid rings forms a more rigid framework. The segmental dynamics of threaded linear chains directly correlates with the microscopic structural packing states. This non-monotonic dependence on coverage is observed consistently in all the dynamical properties of linear chains investigated in our simulations, including the structural relaxation time τ_α, non-Gaussian parameter α_2, and four-point susceptibility χ_4.

In addition, the characteristic diffusion length scale L_R, which is comparable to the size of one ring, divides the diffusion into two distinct regimes. Within this length scale L_R, the dynamics is determined by the local packing structures. In contrast, when the diffusion length scale exceeds L_R, the diffusion can be slowed down by the topological constraints imposed by the mechanical bonds. For example, the diffusion of the entire polyrotaxane, which is significantly larger than L_R, is expected to slow down as the coverage ϕ increases. Furthermore, the topological constraints weaken the intermolecular interactions of polyrotaxane chains while promoting intramolecular cooperative motion. These results are similar to our previous work on supercooled single-chain cross-linked nanoparticle (SCNP) melts.[40] We discovered that intra-chain cross-linking bonds can increase the intramolecular collective motion and decrease the intermolecular collective motion while significantly enhancing dynamic heterogeneity. Therefore, α_2 and χ_4 observed in our simulations exhibit a positive dependence on ϕ at intermediate time scales.

In summary, this research has provided valuable insights into the segmental dynamics of polyrotaxane melts. We have identified the unique structural packing responsible for the anomalous segmental dynamics. These findings have important implications for the design and development of materials based on mechanical interlocking polymers with precisely tailored mechanical properties.

SUPPLEMENTAL MATERIAL

See the supplementary material for the specific volume of particles, density profile for linear/ring monomers, the mean square displacement of monomers of linear chains and rings, the non-Gaussian parameter α_2, and four-point susceptibility χ_4 of linear chains. The simulation source code is provided.

ACKNOWLEDGMENTS

J.Z. acknowledges the support of the National Key R & D Program of China (Grant No. 2022YFE0103800), the National Natural Science Foundation of China (Grant Nos. 21774004 and 22373036). The computation of this work was made possible by the facilities of Information and Network Engineering and Research Center of SCUT.

AUTHOR DECLARATIONS

Conflict of Interest

The authors have no conflicts to disclose.

Author Contributions

Xiang-Meng Jia: Conceptualization (equal); Project administration (equal); Resources (equal); Validation (equal); Visualization (equal); Writing – original draft (equal); Writing – review & editing (equal). **Jiajia Zhou**: Project administration (equal); Resources (equal); Supervision (equal); Writing – review & editing (equal).

DATA AVAILABILITY

The data that support the findings of this study are available from the corresponding author upon reasonable request.

REFERENCES

[1]L. F. Hart, J. E. Hertzog, P. M. Rauscher, B. W. Rawe, M. M. Tranquilli, and S. J. Rowan, "Material properties and applications of mechanically interlocked polymers," Nat. Rev. Mater. **6**, 508–530 (2021).
[2]V. Richards, "Molecular machines," Nat. Chem. **8**, 1090 (2016).
[3]J. F. Stoddart, "Mechanically interlocked molecules (MIMs)—Molecular shuttles, switches, and machines (nobel lecture)," Angew. Chem., Int. Ed. **56**, 11094–11125 (2017).
[4]B. L. Feringa, "The art of building small: From molecular switches to motors (Nobel lecture)," Angew. Chem., Int. Ed. **56**, 11060–11078 (2017).
[5]C.-C. Zhang, Y.-M. Zhang, Z.-Y. Zhang, X. Wu, Q. Yu, and Y. Liu, "Photoreaction-driven two-dimensional periodic polyrotaxane-type supramolecular nanoarchitecture," Chem. Commun. **55**, 8138–8141 (2019).
[6]J. Paulo Coelho, J. Osío Barcina, E. Junquera, E. Aicart, G. Tardajos, S. Gómez-Graña, P. Cruz-Gil, C. Salgado, P. Díaz-Núñez, O. Peña-Rodríguez, and A. Guerrero-Martínez, "Supramolecular control over the interparticle distance in gold nanoparticle arrays by cyclodextrin polyrotaxanes," Nanomaterials **8**, 168 (2018).
[7]S. Uenuma, R. Maeda, H. Yokoyama, and K. Ito, "Formation of isolated pseudo-polyrotaxane nanosheet consisting of α-cyclodextrin and poly(ethylene glycol)," Macromolecules **52**, 3881–3887 (2019).
[8]B. He, Y. Lai, B. He, Y. Li, G. Wang, S. Chang, and Z. Gu, "Supramolecular nanoparticles generated by the self-assembly of polyrotaxanes for antitumor drug delivery," Int. J. Nanomed. **7**, 5249–5258 (2012).
[9]Y. Ji, X. Liu, M. Huang, J. Jiang, Y.-P. Liao, Q. Liu, C. H. Chang, H. Liao, J. Lu, X. Wang, M. J. Spencer, and H. Meng, "Development of self-assembled multi-arm polyrotaxanes nanocarriers for systemic plasmid delivery *in vivo*," Biomaterials **192**, 416–428 (2019).
[10]J. S. W. Seale, Y. Feng, L. Feng, R. D. Astumian, and J. F. Stoddart, "Polyrotaxanes and the pump paradigm," Chem. Soc. Rev. **51**, 8450–8475 (2022).
[11]T. Taharabaru, T. Kihara, R. Onodera, T. Kogo, Y. Wen, J. Li, K. Motoyama, and T. Higashi, "Versatile delivery platform for nucleic acids, negatively charged protein drugs, and genome-editing ribonucleoproteins using a multi-step transformable polyrotaxane," Mater. Today Bio **20**, 100690 (2023).
[12]G.-Z. Yin, J. Hobson, Y. Duan, and D.-Y. Wang, "Polyrotaxane: New generation of sustainable, ultra-flexible, form-stable and smart phase change materials," Energy Storage Mater. **40**, 347–357 (2021).
[13]P. Ding, L. Wu, Z. Lin, C. Lou, M. Tang, X. Guo, H. Guo, Y. Wang, and H. Yu, "Molecular self-assembled ether-based polyrotaxane solid electrolyte for lithium metal batteries," J. Am. Chem. Soc. **145**, 1548–1556 (2023).
[14]K. Mayumi, C. Liu, Y. Yasuda, and K. Ito, "Softness, elasticity, and toughness of polymer networks with slide-ring cross-links," Gels **7**, 91 (2021).
[15]Z. H. Xie, M. Z. Rong, M. Q. Zhang, and D. Liu, "Implementation of the pulley effect of polyrotaxane in transparent bulk polymer for simultaneous strengthening and toughening," Macromol. Rapid Commun. **41**, 2000371 (2020).
[16]K. Kato, A. Ohara, H. Yokoyama, and K. Ito, "Prolonged glass transition due to topological constraints in polyrotaxanes," J. Am. Chem. Soc. **141**, 12502–12506 (2019).
[17]K. Kato, T. Mizusawa, H. Yokoyama, and K. Ito, "Effect of topological constraint and confined motions on the viscoelasticity of polyrotaxane glass with different interactions between rings," J. Phys. Chem. C **121**, 1861–1869 (2017).
[18]K. Kato, T. Mizusawa, H. Yokoyama, and K. Ito, "Polyrotaxane glass: Peculiar mechanics attributable to the isolated dynamics of different components," J. Phys. Chem. Lett. **6**, 4043–4048 (2015).
[19]K. Kato, T. Mizusawa, A. Ohara, and K. Ito, "Direct enhancement of intercomponent interactions in polyrotaxane and its pronounced effects on glass state properties," Chem. Commun. **57**, 12472–12475 (2021).
[20]K. Kato, A. Ohara, K. Michishio, and K. Ito, "Effects of ring size on the dynamics of polyrotaxane glass," Macromolecules **53**, 8910–8917 (2020).
[21]K. Kato, M. Naito, K. Ito, A. Takahara, and K. Kojio, "Freestanding tough glassy membranes produced by simple solvent casting of polyrotaxane derivatives," ACS Appl. Polym. Mater. **3**, 4177–4183 (2021).
[22]S. Uenuma, R. Maeda, K. Kato, K. Mayumi, H. Yokoyama, and K. Ito, "Drastic change of mechanical properties of polyrotaxane bulk: ABA–BAB sequence change depending on ring position," ACS Macro Lett. **8**, 140–144 (2019).
[23]K. Kato, K. Ito, and T. Hoshino, "Fracture process of mechanically interlocked ductile glass under uniaxial tension," Macromolecules **56**, 7358–7365 (2023).
[24]Y. Yasuda, Y. Hidaka, K. Mayumi, T. Yamada, K. Fujimoto, S. Okazaki, H. Yokoyama, and K. Ito, "Molecular dynamics of polyrotaxane in solution investigated by quasi-elastic neutron scattering and molecular dynamics simulation: Sliding motion of rings on polymer," J. Am. Chem. Soc. **141**, 9655–9663 (2019).
[25]Y. Yasuda, M. Toda, K. Mayumi, H. Yokoyama, H. Morita, and K. Ito, "Sliding dynamics of ring on polymer in rotaxane: A coarse-grained molecular dynamics simulation study," Macromolecules **52**, 3787–3793 (2019).
[26]J. H. Mangalara and D. S. Simmons, "Tuning polymer glass formation behavior and mechanical properties with oligomeric diluents of varying stiffness," ACS Macro Lett. **4**, 1134–1138 (2015).
[27]F. Vargas-Lara, B. A. Pazmiño Betancourt, and J. F. Douglas, "Influence of knot complexity on glass-formation in low molecular mass ring polymer melts," J. Chem. Phys. **150**, 101103 (2019).
[28]F. W. Starr, S. Sastry, J. F. Douglas, and S. C. Glotzer, "What do we learn from the local geometry of glass-forming liquids?," Phys. Rev. Lett. **89**, 125501 (2002).
[29]W.-S. Xu, J. F. Douglas, and Z.-Y. Sun, "Polymer glass formation: Role of activation free energy, configurational entropy, and collective motion," Macromolecules **54**, 3001–3033 (2021).
[30]W.-S. Xu, J. F. Douglas, and K. F. Freed, "Influence of cohesive energy on the thermodynamic properties of a model glass-forming polymer melt," Macromolecules **49**, 8341–8354 (2016).
[31]W. L. Merling, J. B. Mileski, J. F. Douglas, and D. S. Simmons, "The glass transition of a single macromolecule," Macromolecules **49**, 7597–7604 (2016).
[32]A. Harada, J. Li, and M. Kamachi, "Preparation and properties of inclusion complexes of polyethylene glycol with α-cyclodextrin," Macromolecules **26**, 5698–5703 (1993).
[33]Y.-L. Zhu, H. Liu, Z.-W. Li, H.-J. Qian, G. Milano, and Z.-Y. Lu, "GALAMOST: GPU-accelerated large-scale molecular simulation toolkit," J. Comput. Chem. **34**, 2197–2211 (2013).

[34]X. Xu, J. F. Douglas, and W.-S. Xu, "Parallel emergence of rigidity and collective motion in a family of simulated glass-forming polymer fluids," Macromolecules **56**, 4929–4951 (2023).
[35]X. Xu, J. F. Douglas, and W.-S. Xu, "Thermodynamic–dynamic interrelations in glass-forming polymer fluids," Macromolecules **55**, 8699–8722 (2022).
[36]D. S. Simmons, M. T. Cicerone, Q. Zhong, M. Tyagi, and J. F. Douglas, "Generalized localization model of relaxation in glass-forming liquids," Soft Matter **8**, 11455 (2012).
[37]T. Q. McKenzie-Smith, J. F. Douglas, and F. W. Starr, "Explaining the sensitivity of polymer segmental relaxation to additive size based on the localization model," Phys. Rev. Lett. **127**, 277802 (2021).
[38]B. A. Pazmiño Betancourt, P. Z. Hanakata, F. W. Starr, and J. F. Douglas, "Quantitative relations between cooperative motion, emergent elasticity, and free volume in model glass-forming polymer materials," Proc. Natl. Acad. Sci, U. S. A. **112**, 2966–2971 (2015).
[39]S. C. Glotzer, V. N. Novikov, and T. B. Schrøder, "Time-dependent, four-point density correlation function description of dynamical heterogeneity and decoupling in supercooled liquids," J. Chem. Phys. **112**, 509–512 (2000).
[40]X.-M. Jia, W.-F. Lin, H.-Y. Zhao, H.-J. Qian, and Z.-Y. Lu, "Supercooled melt structure and dynamics of single-chain nanoparticles: A computer simulation study," J. Chem. Phys. **155**, 054901 (2021).